INTERNATIONAL JOURNAL FOR NUMERICAL METHODS IN FLUIDS, VOL. 11, 769–790 (1990)

FINITE ELEMENT FORMULATION FOR TRANSPORT EQUATIONS IN A MIXED CO-ORDINATE SYSTEM: AN APPLICATION TO DETERMINE TEMPERATURE EFFECTS ON THE SINGLE-WELL CHEMICAL TRACER TEST

Y. J. PARK*
University of Houston, Houston, TX 77004, U.S.A.

H. A. DEANS
University of Wyoming, Laramie, WY 82071, U.S.A.

AND

T. E. TEZDUYAR
University of Minnesota and Minnesota Supercomputer Institute, Minneapolis, MN 55455, U.S.A.

SUMMARY

Heterogeneous equation systems in a pair of coupled co-ordinate systems are solved by a finite element method. The specific physical application studied is the effect of temperature on single-well chemical tracer (SWCT) tests to measure residual oil saturation (volume fraction of immobile oil phase) remaining after waterflooding of an oil reservoir. Since temperature effects are caused by injecting cooler surface fluid down a well into a warm reservoir, the vertical temperature profile in the wellbore as well as the temperature distribution in the porous oil-bearing layer must be considered.

The entire system is modelled to account for the different transport mechanisms. However, it is expedient to divide the connected geometrical region into two model domains. The equations for each submodel are expressed in an appropriate set of co-ordinates. The variational formulation of each model is then discussed.

A significant temperature effect on the estimation of residual oil saturation occurs when the radial temperature and concentration wave propagation speeds in the porous formation are about the same. In this case the temperature gradient is located across the chemical tracer bank, causing the chemical reaction rate to vary radially. The temperature effects are demonstrated for two actual field tests in complex reservoirs.

KEY WORDS Heterogeneous Equations Finite Element Residual Oil Saturation Single-well Chemical Tracer Test

1. INTRODUCTION

The single-well chemical tracer (SWCT) test was developed to measure residual oil saturation (S_{or}) after waterflooding of oil reservoirs. The underlying principle of the SWCT method is the chromatographic separation caused by local distribution of the tracers between flowing and non-flowing fluids. This method had its first field test in 1968 and was patented in 1971.[1] Several field applications of the SWCT method were reported in 1973.[2] The 200 field tests performed to date have proved the practical applicability of the method.

* On leave from Pusan National Institute of Technology, Pusan, Korea.

0271–2091/90/140769–22$11.00

Received November 1989

This method involves three time periods—injection, shut-in and production. During the injection period, a carrier fluid containing a reactive (primary) tracer is injected into the oil-bearing formation through a well. After an appropriate amount of carrier fluid–reactant solution is injected, the solution is pushed away from the well by injection of reactant-free carrier fluid.

The carrier fluid–reactant solution is then permitted to remain at rest in the formation for a shut-in period. During this time, part of the reactant tracer reacts to form a product (secondary) tracer. The fluid is then produced back into the same wellbore from which it was injected. Since the unconsumed reactant and the product have differing partition coefficients between the carrier fluid and the immobile phase, they are chromatographically separated in their passage through the formation during this production period. The amount of separation is quantitatively related to the saturation of the immobile oil phase.

In the field test the concentrations of reactant and product are measured at the point of production and plotted versus the volume produced. These results are matched by computer simulation of the equations governing the tracer behaviour during the three time periods. From the best fit, the relative proportions of mobile and immobile fluids in the formation can be determined.

In actual field SWCT tests the injection fluid temperature at the surface is normally lower than the subterranean reservoir temperature. In some high-temperature reservoir cases the temperature difference can be as much as 180 °F. The injection fluid temperature may not reach the reservoir temperature before entering the formation because of limited heat transfer in the well. This causes cooling near the point of injection.

The rate of the chemical reaction is highly temperature-dependent. According to the Arrhenius kinetics, the reaction rate is exponentially dependent on temperature. The reaction rate in the chilled zone is thus slower than that in the higher-temperature zone. Because of this effect, the product tracer profile may be effectively displaced from the reactant tracer profile towards the high-temperature zone. By accounting for this thermal separation together with the chromatographic separation, the simulation estimate of the residual oil saturation value becomes more reliable. Temperature effects on the ideal model, which is applicable to SWCT tests in relatively homogeneous sandstone formations, were first reported by Tezduyar *et al.*[3]

In contrast to sandstones, the pore structure of carbonate formations is often very heterogeneous. Because of this non-uniformity in flow structure, the local tracer distribution may not attain the equilibrium assumed by the usual theory.

The pore diffusion model proposed by Deans and Carlisle[4] accounts for local concentration gradients by introducing a local (internal) domain at every point in the global (external) domain. This idea was earlier used by Horn[5] to describe transport and flow in a general chromatographic system. The concentration distributions within the external domain are governed by transport equations which have additional source terms determined by the fluxes in the local domain. The interfacial source terms maintain continuity conditions between the two subdomains. The local tracer concentrations are governed by diffusion-dominated partial differential equations in the internal domain. The concentration in the external domain is the boundary condition at the interface of the internal domain for each tracer.

The temperature effects on the pore diffusion model are studied in this work. The thermal diffusivity is normally much larger than the molecular diffusivities in a carbonate pore system, the local temperatures of internal and external domains can be assumed to be equal.

The porous reservoir formation is assumed to be a horizontal layer of uniform thickness. Incompressible radial flow occurs within this layer. The centre plane of the permeable layer is assumed to provide symmetry conditions for the distribution of all unknown variables; thus the upper half of the layer is chosen as the computational domain. The computational domain for the

SWCT test accounting for the heat conduction between over/underburden impermeable layers is shown in Figure 1. The concentrations and temperature at the formation face are required to be known as boundary conditions. The tracer concentrations at this face are assumed to be the injected concentrations at the surface. However, temperature rise of the fluid while flowing down the wellbore cannot be neglected.

The temperature of the fluid in the wellbore is first computed, accounting for the heat gained from the surrounding earth. The wellbore domain is also shown in Figure 1. Incompressible flow in the wellbore is modelled in a 1D space, which again acts as an external (boundary) domain of a 2D (axisymmetric cylindrical, internal) space surrounding the wellbore. The heat flux between the two subdomains is included as a source term in the external domain equation. It is computed from the temperature gradient in the internal domain. The temperature in the external domain is the boundary condition for the internal domain equation at the interface.

The SWCT and wellbore problems are similar, in that the equations are expressed in coupled co-ordinate systems with flux terms in the external domain and boundary conditions for the internal domain. The difference between the two problems is in the nature of the internal domains. The internal domain for the wellbore problem is a simply connected region and the external domain is one surface of the internal domain. However, the external domain in the pore diffusion model surrounds an infinite number of independent internal domains, each of which communicates only with the external domain at the point where the local domain is defined.

2. THE PROBLEM STATEMENT

Consider a domain Ω consisting of several subdomains; the space dimensions and even the co-ordinate systems for the different subdomains may not be same. The entire domain is an assembly

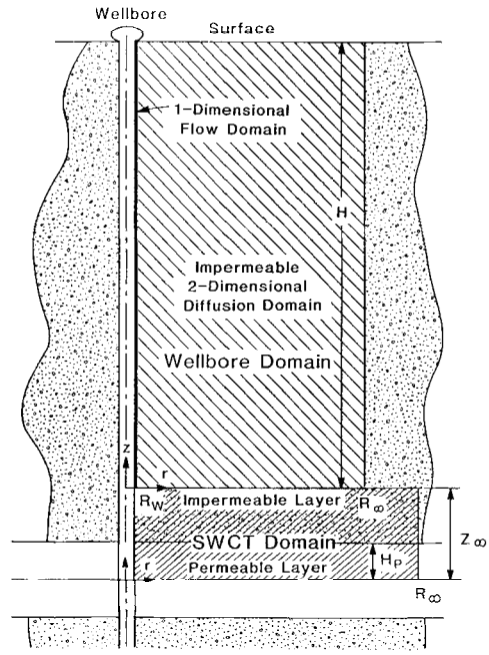

Figure 1. The geometry and the computational domains

of the subdomains involved, i.e.

$$\bar{\boldsymbol{\Omega}} = \{\bar{\Omega}^{(\mu)} \text{ of } \mathscr{R}^{n_{sd}^{(\mu)}}\}_{\mu=1,\ldots,n_{mat}}, \tag{1}$$

where n_{mat} is the number of subdomains and $n_{sd}^{(\mu)}$ is the number of space dimensions for $\Omega^{(\mu)}$. The superscript μ, which is the index for the subdomain number, is parenthesized. The conventions for the superscripts and subscripts used throughout this work are given in Appendix II.

For the case when the co-ordinate systems for the subdomains are not equal, the spatial co-ordinates for each subdomain must be defined individually:

$$\mathbf{x}^{(\mu)} \in \bar{\Omega}^{(\mu)}. \tag{2}$$

However, the time co-ordinate for investigating concurrent behaviour of the unknown variables is uniquely defined by

$$t \in [0, t_{max}]. \tag{3}$$

Consider the following vector partial differential equation governing the behaviour of the dependent variables:

$$(1+\beta)\partial\psi/\partial t + \mathbf{u}\cdot\nabla\psi - \nabla\cdot(\gamma\nabla\psi) + \mathbf{R} = \mathbf{F} \quad \text{on } \boldsymbol{\Omega}. \tag{4}$$

A vector of unknown variables, ψ, is defined by using two superscripts as follows:

$$\psi = \{\psi^{I(\mu)}\}_{I=I_{dofb}^{(\mu)},\ldots,I_{dofe}^{(\mu)},\ \mu=1,\ldots,n_{mat}}, \tag{5}$$

where I is the counter for the dependent variable in the subdomain μ, and $I_{dofb}^{(\mu)}$ and $I_{dofe}^{(\mu)}$ are the beginning and end counts for the dependent variables in the μth subdomain. These counts are introduced to avoid confusion in the numbering of the dependent variables, especially for the pore diffusion model.

An internal subdomain $\Omega^{(\mu)}$ may be an assembly of independent spaces as given by

$$\boldsymbol{\Omega}^{(\mu)} = \{\Omega_k^{(\mu)}\}_{k=1,\ldots,n_{pl}}, \tag{6}$$

where n_{pl} is the number of independent spaces in $\Omega^{(\mu)}$.

The number of space dimensions and the number of unknown variables in each subdomain, and the nature of the internal subdomain, are discussed for each model, along with the initial and boundary conditions.

Remark 1. The subdomain $\Omega^{(1)}$ is designated to be the external subdomain. An interfacial source term $\mathbf{F}$ appears in the subdomain equations in order to maintain the continuity conditions for the distribution of dependent variables between the two subdomains. The term $\mathbf{F}$ vanishes in the equations for the internal subdomains.

The wellbore model

The internal subdomain $\Omega^{(2)}$ in this model is a connected region of $\mathscr{R}^2$ representing the earth surrounding a wellbore, and the wellbore is the external subdomain $\Omega^{(1)}$. The entire domain is composed of two subdomains, i.e.

$$\boldsymbol{\Omega} = \Omega^{(1)} \cup \Omega^{(2)}. \tag{7}$$

These subdomains are

$$\Omega^{(1)} = \{z \mid z \in [0, H]\}, \tag{8}$$

$$\Omega^{(2)} = \{(r, z) \mid r \in [R_w, R_\infty], \quad z \in [0, H]\}, \tag{9}$$

where H is the height of the wellbore domain, R_w is the radius of the wellbore and R_∞ is the radial co-ordinate at the boundary of the computational domain; R_∞ should be large enough to be beyond the influence of the wellbore cooling. The numbering of the subdomains, the various media involved and the dependent variables are shown in Table I. The dependent variable vector in this model is given by

$$\psi = \begin{Bmatrix} \psi^{1(1)} \\ \psi^{1(2)} \end{Bmatrix} = \begin{Bmatrix} T(z) \\ T(r, z) \end{Bmatrix}. \tag{10}$$

The non-zero terms in equation (4) for the wellbore model are shown in Appendix I. The initial temperature distribution assumes a constant geothermal gradient g_T, i.e.

$$T = T(z) = T_s + g_T(H - z), \tag{11}$$

where T_s is the earth surface temperature.

The boundary conditions are

$$T = T_s \quad \text{at } z = H \quad \text{on } \Omega^{(1)} \text{ and } \Omega^{(2)}, \tag{12}$$

$$\partial T/\partial z = 0 \quad \text{at } z = 0 \quad \text{on } \Omega^{(1)} \text{ and } \Omega^{(2)}, \tag{13}$$

$$\psi^{1(2)} = \psi^{1(1)} \quad \text{at } r = R_w \quad \text{on } \Omega^{(2)}, \tag{14}$$

$$T = T_E(z) \quad \text{at } r = R_\infty \quad \text{on } \Omega^{(2)}, \tag{15}$$

where $T_E(z)$ is the earth temperature given by equation (11).

The pore diffusion model

The external subdomain in this model is a subset of $\mathscr{R}^2$ and is composed of two subdomains: (1) flowing fraction of the permeable layer and (2) the impermeable layer. Temperature is the only unknown variable in the impermeable layer, and is governed heat conduction. Both temperature and tracer concentrations are unknown in the permeable layer.

Subdomains 1 and 2 represent the flowing fraction of the permeable layer and the impermeable layer respectively; the co-ordinates $\mathbf{x}^{(1)} \in \bar{\Omega}^{(1)}$ and $\mathbf{x}^{(2)} \in \bar{\Omega}^{(2)}$ are of the same axisymmetric system. Coupling of equations in the mixed co-ordinate system occurs between $\Omega^{(1)}$ and $\Omega^{(3)}$. The external domains are defined by

$$\Omega^{(1)} = \{(r, z) | r \in [R_w, R_\infty], z \in [0, H_p]\}, \tag{16}$$

$$\Omega^{(2)} = \{(r, z) | r \in [R_w, R_\infty], z \in [H_p, Z_\infty]\}, \tag{17}$$

where H_p is the half-height of the permeable layer and R_∞, Z_∞ are the radial and axial co-ordinates at the computational boundaries.

Table I. The numbering of the subdomains, the various media involved and the dependent variables for the wellbore model

Domain	Subdomain	Medium	Subdomain number	Dependent variable number
				1
Ω	$\Omega^{(1)}$ of $\mathscr{R}^1$	Wellbore	1	T
	$\Omega^{(2)}$ of $\mathscr{R}^2$	Surrounding earth	2	T

The internal subdomain which represents the dead-end pores in the permeable layer is an assembly of many independent spaces $\Omega_k^{(3)}$ (which are all subsets of $\mathscr{R}^1$) as shown by expression (6). Each domain is assumed to have an average length l and is attached at a particular node in the flowing fraction of the permeable layer. Therefore the domains are given as $\Omega_k^{(3)}$, $k=1, \ldots, n_{\mathrm{pl}}$, where n_{pl} is the number of nodal points in the permeable layer. The co-ordinates for these dead-end pore subdomains are

$$\Omega^{(3)}=\{y_k \mid y_k \in [0, l], k=1, \ldots, n_{\mathrm{pl}}\}. \tag{18}$$

The temperature at each stagnant pore is assumed to be equal to the temperature at the flowing part where the pore is attached, i.e.

$$T(r, z, t, y)=T(r, z, t) \quad \forall y \in [0, l]. \tag{19}$$

This can be justified in heterogenieties of centimetre size scale, typical of carbonate pore structures, because of their large thermal conductivity.[6, 7] Temperature is thus eliminated as a dependent variable in these subdomains. The numbering of the subdomains, the various media involved and the dependent variables are shown in Table II. The complete set of dependent variables in the entire domain is given by

$$\psi=\begin{Bmatrix} \psi^{I(1)} \\ \psi^{I(2)} \\ \psi^{I(3)} \end{Bmatrix}=\begin{Bmatrix} \begin{pmatrix} \psi^{1(1)} \\ \psi^{2(1)} \\ \psi^{3(1)} \end{pmatrix} \\ (\psi^{1(2)}) \\ \begin{pmatrix} \psi^{2(3)} \\ \psi^{3(3)} \end{pmatrix} \end{Bmatrix}=\begin{Bmatrix} \begin{pmatrix} T \\ C^{\mathrm{A}} \\ C^{\mathrm{B}} \end{pmatrix} \\ (T) \\ \begin{pmatrix} C^{\mathrm{A}} \\ C^{\mathrm{B}} \end{pmatrix} \end{Bmatrix}. \tag{20}$$

Note that the dependent variable count for subdomain 3 starts with 2. The number 1 is assigned to the temperature, which is equal to the external domain temperature according to equation (19). Each dependent variable thus has an equivalent number throughout the entire domain. However, additional indices, the beginning and end counts, have been used to keep this numbering in order, as shown in Table III.

The non-zero components of the velocity vectors are the radial velocities in the flowing fraction of the permeable layer (i.e. $u_1^{i(1)}$). However, since the equilibrium model used for the temperature is different from the model applied to the concentrations, their velocities differ. The term **R** in

Table II. The numbering of the subdomains, the various media involved and the dependent variables for the pore diffusion model

Domain	Subdomain	Medium	Subdomain number	Dependent variable number		
				1	2	3
Ω	$\Omega^{(1)}$ of $\mathscr{R}^2$	Flowing fraction	1	T	C^{A}	C^{B}
	$\Omega^{(2)}$ of $\mathscr{R}^2$	Impermeable layer	2	T		
	$\Omega^{(3)}$ of $\mathscr{R}^1$	Stagnant fraction	3		C^{A}	C^{B}

Table III. Beginning and end counts for dependent variables

	The wellbore model		The pore diffusion model		
	Material number		Material number		
	1	2	1	2	3
$I^{(\mu)}_{\text{dofb}}$	1	1	1	1	2
$I^{(\mu)}_{\text{dofe}}$	1	1	3	1	3

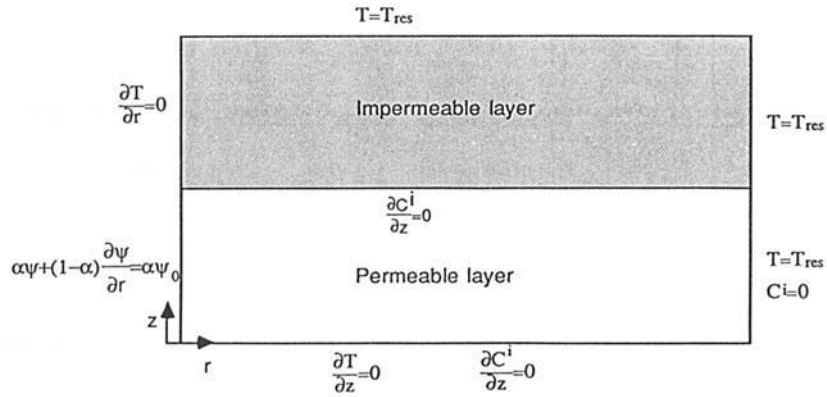

Figure 2. Boundary conditions for the SWCT domain: $\alpha=1$, injection period; $\alpha=0$, shut-in and production periods

equation (4) represents the source (or sink) due to the chemical reaction A→B. The velocity field and all the coefficients in equation (4) are described in Appendix I.

The original reservoir conditions are used as the initial conditions for the entire domain. The boundary conditions for the external subdomain are shown in Figure 2. The boundary conditions for the internal subdomains are

$$\psi^{I(3)}(r, z, t, y) = \psi^{I(1)}(r, z, t) \quad \text{at } y=0, \tag{21}$$

$$\partial\psi^{I(3)}/\partial y=0 \quad \text{at } y=l. \tag{22}$$

3. THE FINITE ELEMENT FORMULATION

In the discretization of Ω into element subdomains Ω^e, $e=1, 2, \ldots, n_{\text{el}}$, only one set of elements is used regardless of which $\Omega^{(\mu)}$ the element Ω^e belongs to. Therefore n_{el} is the total number of elements in the entire domain Ω. It is assumed that

$$\bar{\Omega} = \bigcup_{e=1}^{n_{\text{el}}} \bar{\Omega}^e, \tag{23}$$

$$\varnothing = \bigcup_{e=1}^{n_{\text{el}}} \bar{\Omega}^e. \tag{24}$$

Let $\mathscr{V}^{I(\mu)}$ and $\mathscr{S}^{I(\mu)}$ denote the weighting and trial solution function spaces for the subdomain $\Omega^{(\mu)}$:

$$\mathscr{V}^{I(\mu)} = \{w^{I(\mu)} | w^{I(\mu)} \in H^1(\Omega), \quad w^{I(\mu)}(\mathbf{x}) = 0, \quad \text{on} \quad \mathbf{x} \in \Gamma^{(\mu)}_{g^{I(\mu)}}\}, \tag{25}$$

$$\mathscr{S}^{I(\mu)} = \{\psi^{I(\mu)} | \psi^{I(\mu)} \in H^1(\Omega), \quad \psi^{I(\mu)}(\mathbf{x}) = g^{I(\mu)}, \quad \text{on} \quad \mathbf{x} \in \Gamma^{(\mu)}_{g^{I(\mu)}}\}, \tag{26}$$

where Γ represents the boundary and g denotes a Dirichlet-type boundary condition. The variational form of equation (4) satisfying the boundary conditions and the associated initial conditions is given as follows:

$$(W) = \begin{cases} \text{given } g^{I(\mu)}, h^{I(\mu)} \text{ and } \psi_0^{I(\mu)}, \text{ find } \psi^{I(\mu)} \in \mathscr{S}^{I(\mu)}, t \in [0, t_{\max}], \\ \text{such that for all } w^{I(\mu)} \in \mathscr{V}^{I(\mu)} \\ \displaystyle\int_{\Omega^{(\mu)}} [w^{I(\mu)}(1+\beta^{I(\mu)})\partial\psi^{I(\mu)}/\partial t + w^{I(\mu)}\mathbf{u}^{I(\mu)} \cdot \nabla^{(\mu)}\psi^{I(\mu)} \\ + \nabla^{(\mu)} w^{I(\mu)} \cdot \gamma^{I(\mu)} \nabla^{(\mu)} \psi^{I(\mu)} + w^{I(\mu)} R^{I(\mu)} - w^{I(\mu)} F^{I(\mu)}] \, \mathrm{d}\Omega^{(\mu)} \\ = \displaystyle\int_{\Gamma_{h^{I(\mu)}}} w^{I(\mu)} h^{I(\mu)} \, \mathrm{d}\Gamma^{(\mu)}, \quad I = I^{(\mu)}_{\text{dofb}}, \ldots, I^{(\mu)}_{\text{dofe}}, \\ \displaystyle\int_{\Omega^{(\mu)}} w^{I(\mu)} (\psi^{I(\mu)} - \psi_0^{I(\mu)}) \, \mathrm{d}\Omega^{(\mu)} = 0, \quad I = I^{(\mu)}_{\text{dofb}}, \ldots, I^{(\mu)}_{\text{dofe}}. \end{cases} \tag{27}$$

The treatment of the flux term in the variational formulation is described for each model. The streamline–upwind/Petrov–Galerkin weighting functions used in this work are described elsewhere.[3,8] A predictor/multicorrector algorithm[9] is used for time integration.

The wellbore model

Since the wellbore domain $\Omega^{(1)}$ is a part of the boundary of $\Omega^{(2)}$, $\Omega^{(1)}$ can be called Γ^1 and $\Omega^{(2)}$ can be simplified to Ω. Temperature is the only dependent variable which covers the entire domain, thus the superscript I and the subdomain number 2 may be dropped without ambiguity. The boundary of the boundary domain Γ^1 is denoted by Γ^Γ and is decomposed as

$$\Gamma^\Gamma = \overline{\Gamma^\Gamma_g \cup \Gamma^\Gamma_h}, \tag{28}$$

$$\varnothing = \Gamma^\Gamma_g \cap \Gamma^\Gamma_h. \tag{29}$$

The boundary conditions are given by equations (12) and (13). On the other hand, the boundary Γ of the domain Ω is assumed to be decomposed as

$$\Gamma = \overline{\Gamma^1 \cup \Gamma_g \cup \Gamma_h}, \tag{30}$$

$$\varnothing = \Gamma^1 \cap \Gamma_g = \Gamma_g \cap \Gamma_h = \Gamma_h \cap \Gamma^1. \tag{31}$$

The boundaries Γ_g and Γ_h admit the Dirichlet- and Neumann-type boundary conditions given by equations (12)–(15). The boundary condition (14) indicates that the temperature on Γ^1 is controlled only by the equation on Γ^1. Therefore the weighting function on Ω is required to be zero along Γ^1, i.e.

$$w = 0 \quad \text{on } \Gamma^1. \tag{32}$$

The flux term in the variational formulation (27) is a boundary integration which can be rewritten by using the divergence theorem,

$$\int_{\Gamma^1} w^1 \gamma \nabla\psi \cdot \mathbf{n}\, d\Gamma^1 = \int_\Omega \nabla\cdot(w^\Omega \gamma\nabla\psi)\, d\Omega = \int_\Omega \nabla w^\Omega \cdot(\gamma\nabla\psi)\, d\Omega + \int_\Omega w^\Omega \nabla\cdot(\gamma\nabla\psi)\, d\Omega, \tag{33}$$

where w^Ω denotes the lifting of w^1 on Ω and $\mathbf{n}$ is the outward unit normal vector on Γ^1. The weighting function w^Ω is required to vanish along all boundaries except Γ^1. The last term in equation (33) can be replaced using equation (4). Since both weighting functions w and w^Ω are chosen from the same space (H^1), w^Ω is the complementary weighting function along Γ^1. By redefining the weighting functions as

$$\mathscr{V} = \{w \mid w \in H^1(\Omega), \quad w = 0 \quad \text{on } \Gamma_g \quad \text{and } \Gamma_g^\Gamma\}, \tag{34}$$

the weak form for the whole domain becomes

$$(W) = \begin{cases} \text{given } g, h \text{ and } \psi_0 \text{ find } \psi \in \mathscr{S}, t \in [0, T], \quad \text{such that for all } w \in \mathscr{V} \\ a\left(\displaystyle\int_\Omega [w(1+\beta)\partial\psi/\partial t + w\mathbf{u}\cdot\nabla\psi + \nabla w\cdot\gamma\nabla\psi + wR]\, d\Omega\right) \\ + \displaystyle\int_{\Gamma^1} [w(1+\beta^1)\partial\psi/\partial t + w\mathbf{u}^1\cdot\nabla^1\psi + \nabla^1 w\cdot\gamma^1\nabla^1\psi + wR^1]\, d\Gamma^1 \\ = a\displaystyle\int_{\Gamma_h} wh\, d\Gamma + \int_{\Gamma_h^\Gamma} wh^\Gamma\, d\Gamma^\Gamma, \\ \displaystyle\int_\Omega w(\psi - \psi_0)\, d\Omega = 0, \end{cases} \tag{35}$$

where a is the interfacial area per unit volume of wellbore between the two subdomains, which, for cylindrical co-ordinates, is equal to $2/R_w$. The spatial discretization of the variational formulation (35) can be performed by a standard finite element procedure.

The pore diffusion model

This model assumes that the internal domains are uniformly distributed in the flowing fraction of the permeable layer. In the numerical approximation an associated subdomain $\Omega^{(3)}$ is attached to every node in the external domain in the permeable layer ($\Omega^{(1)}$). Therefore the number of independent subdomains in $\Omega^{(3)}$ is the same as the number of nodes in $\Omega^{(1)}$. A finite element mesh which contains the one-dimensional subdomains is shown in Figure 3. It is also assumed that the contribution of each space in $\Omega^{(3)}$ is limited to the corresponding node in $\Omega^{(1)}$. That is, there is no cross-diffusion between adjacent spaces in $\Omega^{(3)}$.

The weak formulation used in the wellbore model was not used in here because of the cross-contributions which occur in the formulation of the flux term. In order to remove the cross-contributions, the projection of the interpolation function of a given node in $\Omega^{(3)}$ on $\Omega^{(1)}$ is assumed to be a delta function whose area is equivalent to the integration of the associate flux term over $\Omega^{(1)}$. Thus the flux term becomes

$$\int_{\Omega^{(1)}} w^{I(1)} a\gamma^{I(3)} \nabla^{(3)} \psi^{I(3)} \cdot \mathbf{n}\, d\Omega^{(1)} \approx \left(\int_{\Omega^{(1)}} w^{I(1)} a\gamma^{I(3)}\, d\Omega^{(1)}\right)\left(\frac{\partial\psi^{I(3)}}{\partial y}\right)_{y=0}, \tag{36}$$

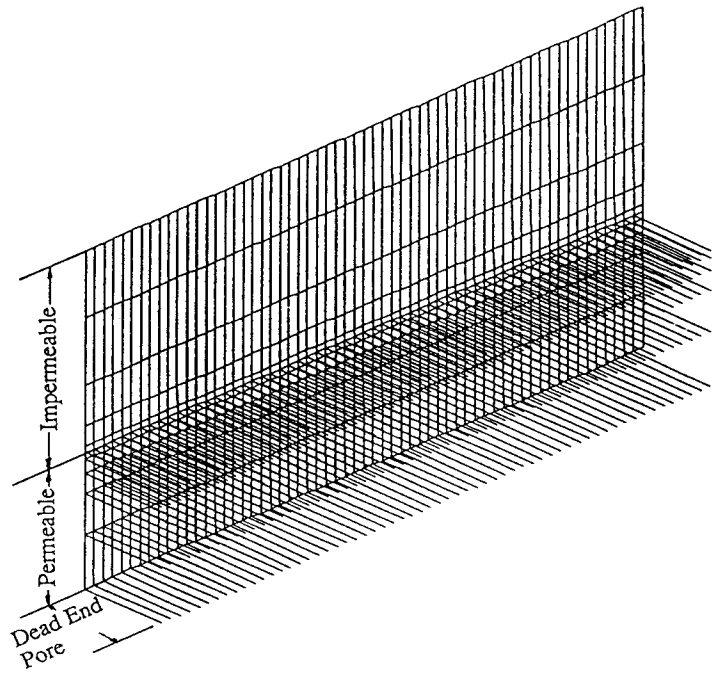

Figure 3. The finite element mesh used in the pore diffusion model ($60 \times 10 + 60 \times 6 \times 5$ elements)

where a is the interfacial area per unit volume between $\Omega^{(1)}$ and $\Omega^{(3)}$, given by

$$a = \frac{f(1-S_o^{(3)})}{l(1-f)(1-S_o^{(1)})}. \tag{37}$$

The y-axis is assumed to be orthogonal to the r–z plane. The correct weight of the flux term in the differential equation can be maintained in the discretized formulation using this approach.

In the finite element discretization the interpolation function associated with a nodal point 'A' (i.e. N_A) is piecewise continuous and the value of N_A is zero on the entire domain except for the elements sharing the node A. In the numbering of nodes, only one sequence is used regardless of which subdomain the node belongs to. Therefore nodal values of the dependent variables can be interpolated by the finite element interpolation rule over the entire domain. At this point one can see that the computation of the element level matrices and vectors can easily be performed by defining the element domain. It is worth mentioning that the spatial dimensions of the subdomains may differ from each other. Therefore the shape functions, the integration rules, the number of dependent variables and the coefficients involved in the equations all depend on the element domain. Moreover, each node in $\Omega^{(1)}$ includes the contributions of a branch in $\Omega^{(3)}$ in order to compute the flux term. As long as these are kept track of along with the element subdomains, the weak form can be discretized using a consistent finite element approach.

Remark 2. The heat of reaction is neglected in this problem because of the low concentration of the reactive tracer and the slow reaction rate. The heat equation is independent of the concentration equations but the concentrations are temperature-dependent. Thus the temperature equation is solved first at every time step. Once the temperature at every node is determined, the first-order reaction rate can be calculated. The mass balance equations, which are linear, can then be solved.

Remark 3. The assembly of the global matrices for the heat equation over $\Omega^{(1)}$ and $\Omega^{(2)}$ is straightforward. However, the assembly of the global matrices for the mass balance equations is worth illustrating. For example, a 12-node mesh consisting of one external domain element and our branches for dead-end pores is shown in Figure 4. In this figure the sequences of numbers (1), (2), . . . , (12) and 1, 2, . . . , 24 stand for the node and equation numbers respectively. The global matrix resulting from the finite element formulation of the tracer equations is shown in Figure 5.

4. RESULTS

The variational formulations of the two submodels (wellbore and pore diffusion models) were coded into computer programs. The behaviour of the dependent variables was then computed in the entire spatial and time domain for several examples. Appropriate data obtained from reservoir and SWCT operating conditions were used for the computation (see references 3, 6 and 7 for details).

In the wellbore model, only the injection period of the SWCT needs to be considered to provide the required boundary condition for the fluid injection into the formation.

Several aspects of tracer behaviour in the pore diffusion model are first investigated by computer simulations. Two field tests are then matched to find the best-fit parameters, including the residual oil saturation value. This is the primary objective of the field test.

Results for the wellbore model

Figure 6 shows the temperature contour lines in the wellbore domain after two days of injection. The initial contours were the horizontal lines given by equation (11). The horizontal

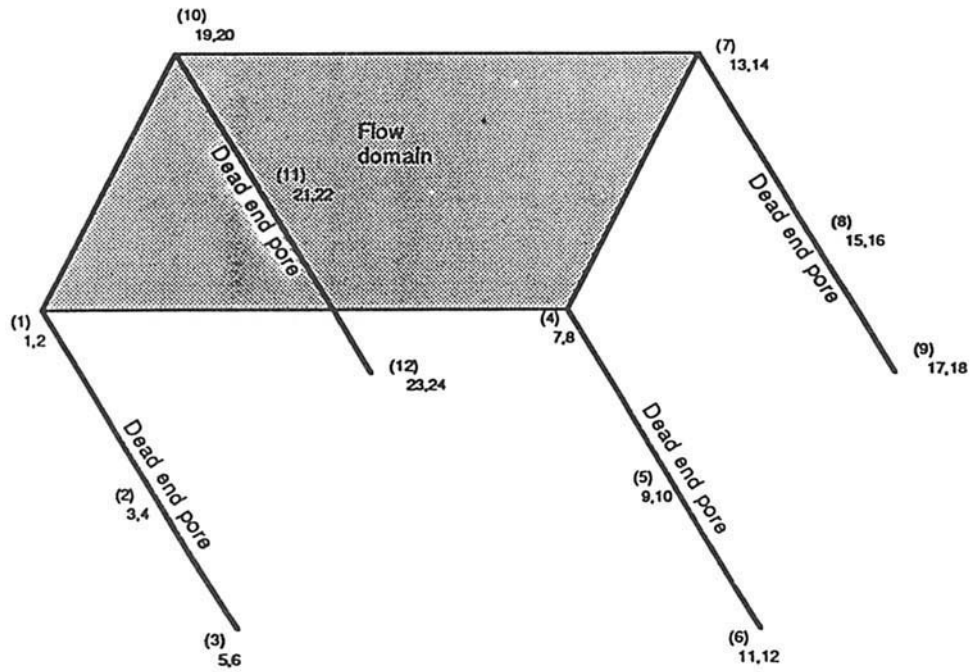

Figure 4. An example mesh to illustrate the assembly of the global matrix for the pore diffusion model

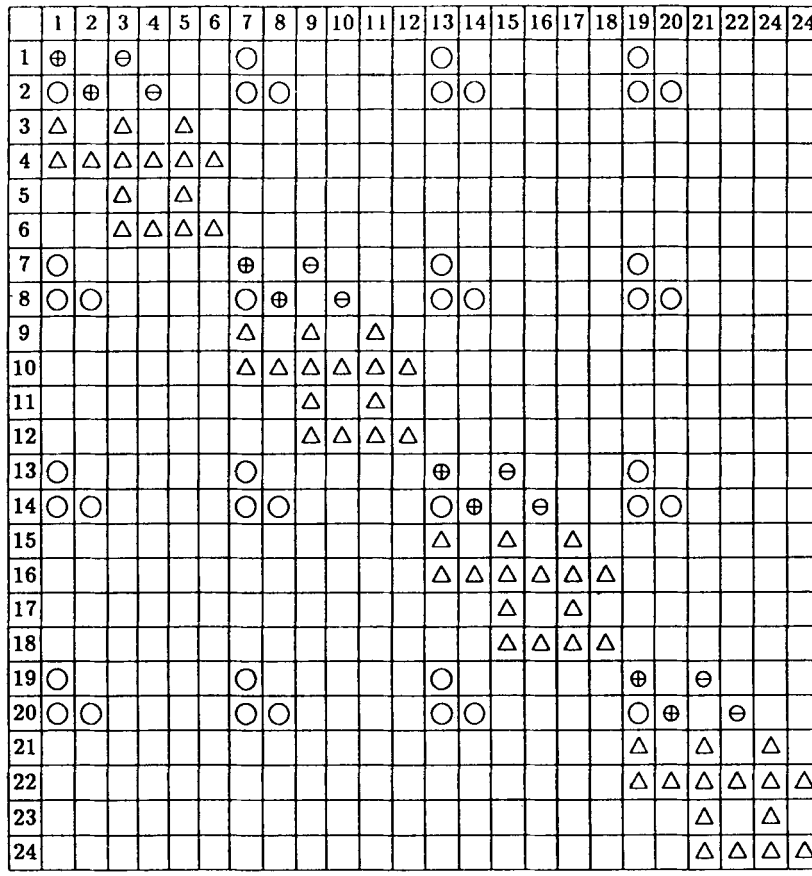

Figure 5. The global matrix for the pore diffusion model equations corresponding to Figure 4: ○; contributions from the flow domain equations (excluding the flux term); ⊕; contributions from the flow domain equations (including the flux term); ⊖; contributions from the flux term in the flow domain; △; contributions from the stagnant domain equations

parts of the contours represent initial conditions, where the effect of the injection fluid has not penetrated. The wellbore region includes tubing, annulus fluid and cement as well as the formation. These materials have different effective thermal conductivities. This material layering was represented in the computational domain by different vertical layers of elements, each of which has its own thermal conductivity. The small horizontal segments in the contour lines adjacent to the wellbore were produced by using a large thermal conductivity in the layer representing fluid inside the casing.

The temperature versus time plot shown in Figure 7 represents the temperature history at the formation, $r = R_w$ and $z = 0$, during the injection. The initial temperature was 208 °F. The surface water temperature was 38 °F. This temperature history is the maximum possible temperature, since the heat transfer coefficient in the casing fluid is assumed to be very large. If the heat transfer coefficient is assumed to be zero, the injection temperature will drop rapidly to the surface injection temperature and remain constant. If field data for the temperature history at the formation are available, the heat transfer coefficient can be estimated by matching the results

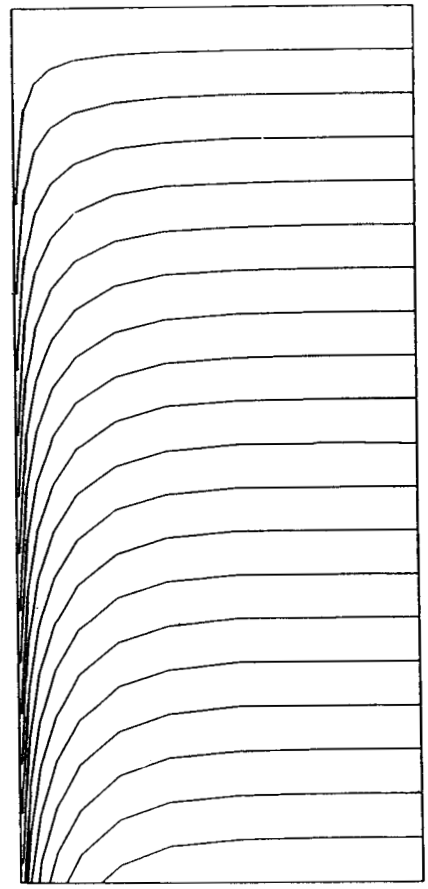

Figure 6. Temperature contour lines around the wellbore (after two days of injection)

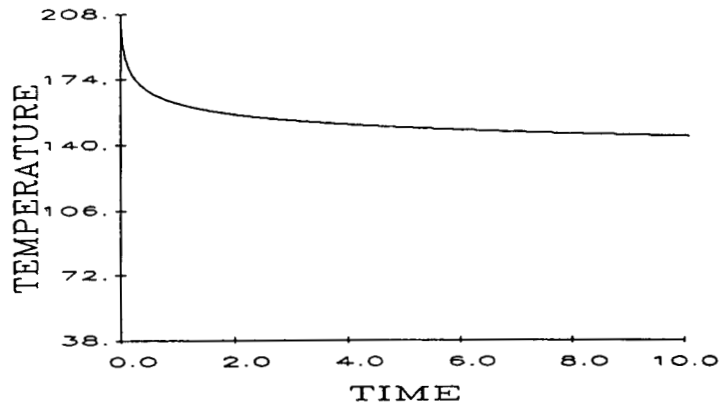

Figure 7. Outflowing fluid temperature at the reservoir permeable layer face

numerically. An estimation of the effective height of the porous layer by matching the temperature history was discussed by Tezduyar *et al.*[3]

It is our purpose to determine realistic temperature behaviour in SWCT tests in order to estimate reliable S_{or}-values. However, no measured temperature history for an SWCT test is available at this time. A lower bound on temperature effects can be evaluated by using the minimum temperature differences between the reservoir and the injected fluid. Therefore the temperature history in Figure 7 has been used as the boundary condition at the wellbore for the SWCT simulations given below.

Results for the pore diffusion model

The reactant tracer distributions in the dead-end pore space at various times are shown in Figure 8. The columns of figures show, from left to right, the distributions at the end of injection, at the end of the shut-in period and after 65% of the injection volume has been produced. Various values of the tracer diffusivity in the dead-end pore spaces ($\gamma^{2(3)}$) are represented in the different rows. With a large $\gamma^{2(3)}$-value the tracer distribution reaches equilibrium between external and

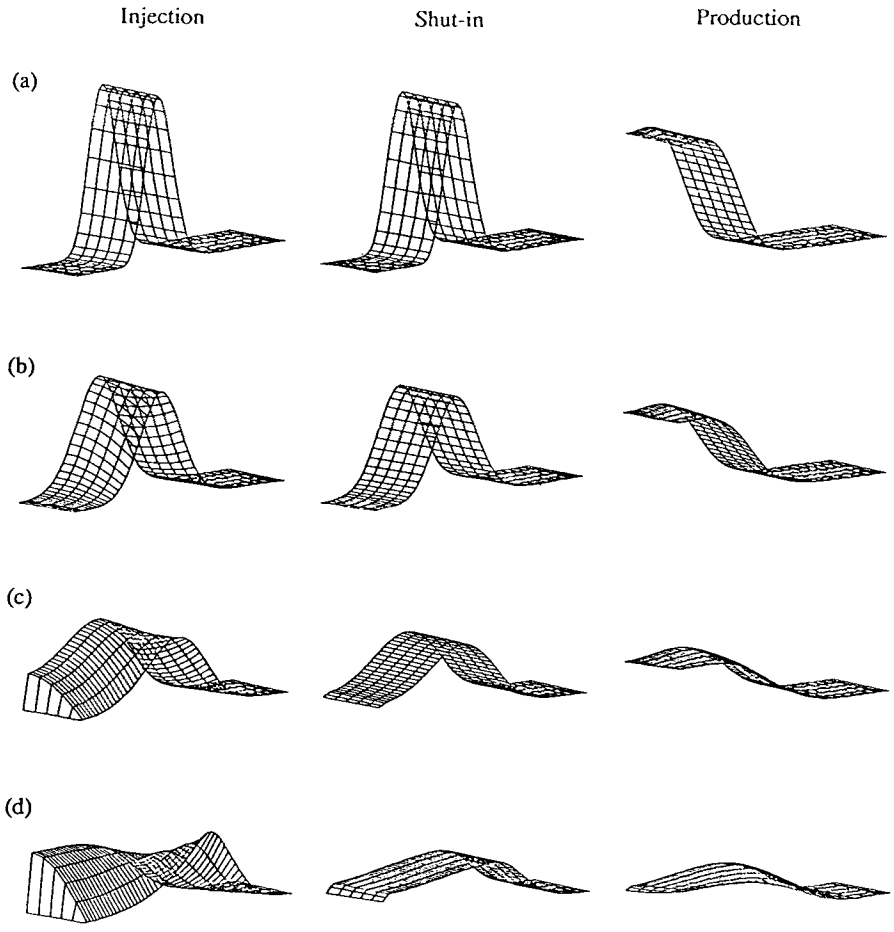

Figure 8. (Continued)

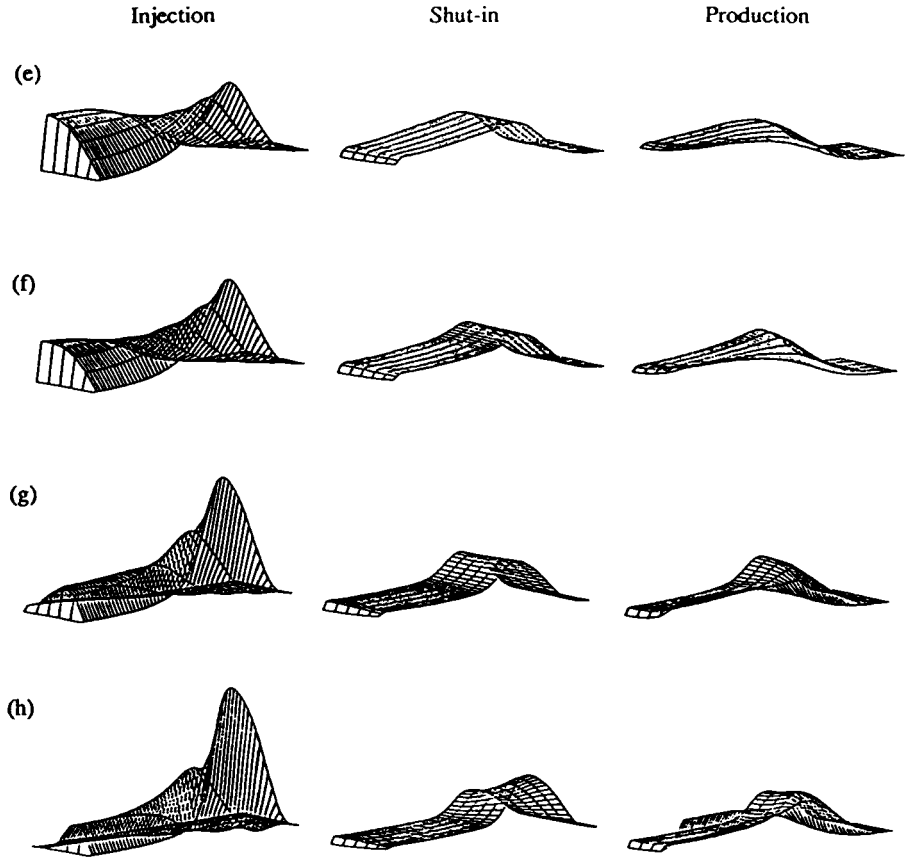

Figure 8. Primary tracer distributions in the dead-end pore spaces: (a) $\gamma = 1000$; (b) $\gamma = 10$; (c) $\gamma = 3{\cdot}0$; (d) $\gamma = 1{\cdot}0$; (e) $\gamma = 0{\cdot}8$; (f) $\gamma = 0{\cdot}5$; (g) $\gamma = 0{\cdot}2$; (h) $\gamma = 0{\cdot}1$

internal spaces. The effects of trapping and releasing of the tracer concentration distribution by the dead-end pore spaces are systematically shown in this collection of pictures. The tracer hold-up and dispersion due to the dead-end pores causes distorted tracer profiles to appear in the production fluid. For intermediate values of γ[2(3)], non-ideal effects such as early arrival of poorly defined peaks, long tails and poor material balance are observed. These effects are commonly found in SWCT field data in carbonate formations.

Figure 9 shows the effect of temperature variation on the relative location of the reactant and product tracers. The wave propagation speeds of temperature and concentration vary with the accumulation capacities of the medium for the respective dependent variables. These capacities are determined by reservoir and operation conditions such as residual oil saturation, rock porosity, heat capacity of rock, and tracer partition coefficients between oil and water phases.

When the speeds of the two fronts are almost the same, the temperature gradient and the tracer bank overlap. Because the reaction rate at high temperature is faster than that at low temperature, the concentration profile of the product tracer (C^B) is displaced towards the high-temperature zone (as seen in Figure 9(a)). Figure 9(b) shows the other case, in which the wave propagation speed of tracer A is faster than that of temperature. The reactant tracer has been

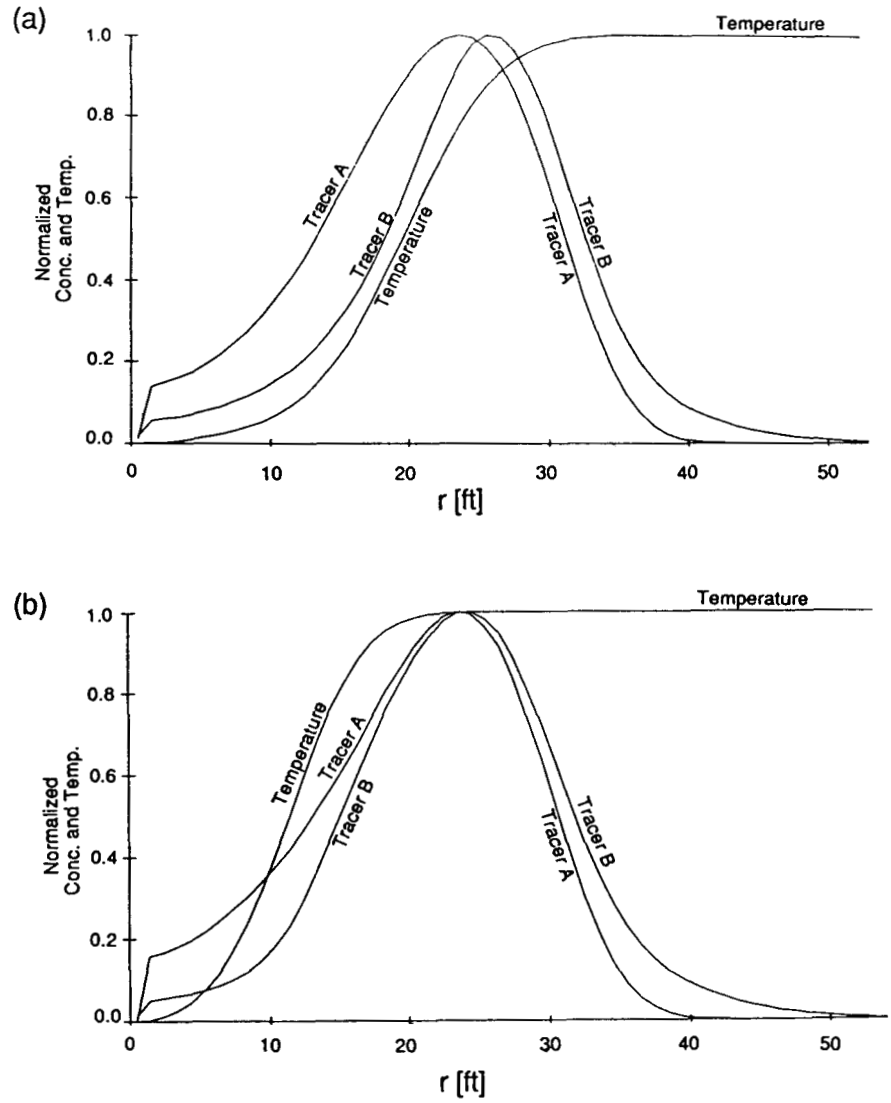

Figure 9. Temperature and tracer profiles at the end of the shut-in period: (a) with significant temperature effect; (b) with negligible temperature effect

pushed into the zone of the original reservoir temperature. The small separation of tracer concentrations shown in Figure 9(b) is due to the reaction which occurred during injection. In this case the temperature effect on the estimation of S_{or} is negligible.

Next the arrival times of the peaks of tracer concentrations are compared between non-isothermal and isothermal simulations. The arrival time of tracer A (Figure 10(a)) varies with dead-end pore diffusivity. It arrives early in the intermediate range of γ (0·5–5·0) for both cases. The peak of tracer B also arrives earlier in the isothermal simulation, but arrives later for the non-isothermal simulation, as shown in Figure 10(b). The difference in the arrival time of tracer B between non-isothermal and isothermal simulations for a given γ-value indicates the magnitude of the temperature effect.

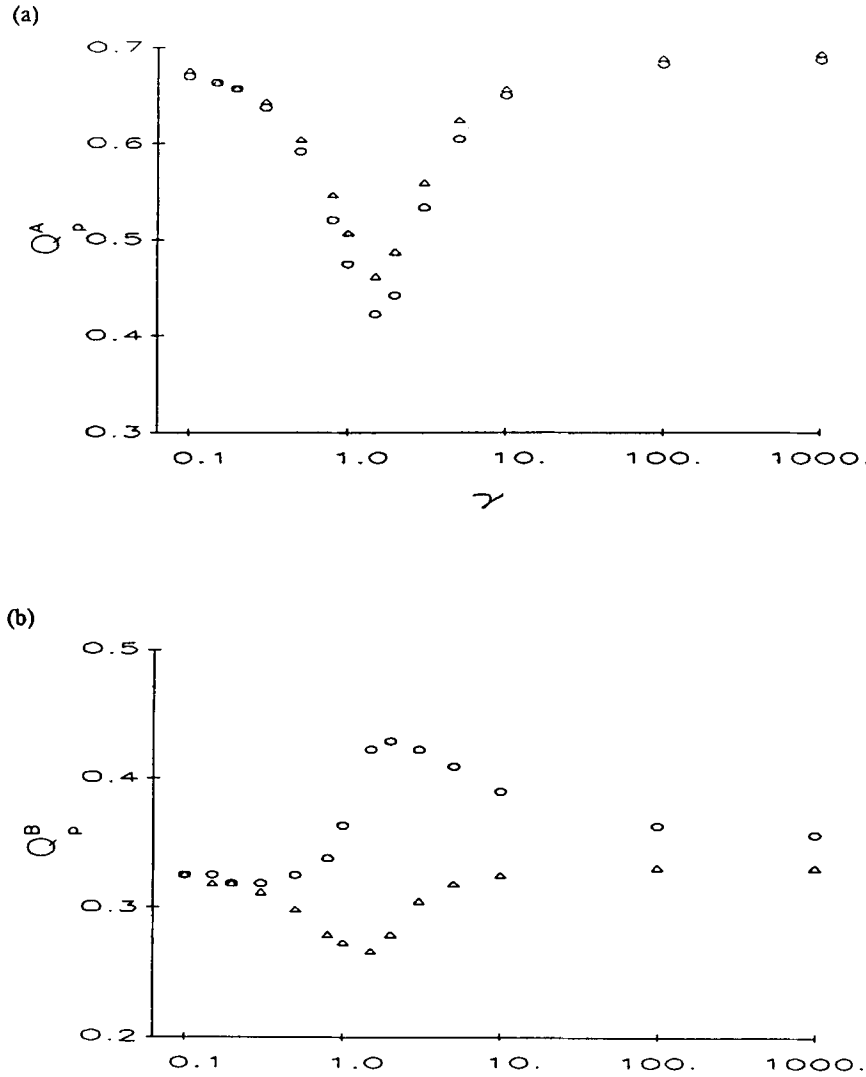

Figure 10. Arrival time of the peak positions ($f=0{\cdot}7$): (a) tracer A; (b) tracer B; ○, non-isothermal; △, isothermal

Criteria which indicate whether an SWCT test is subject to significant temperature effects in the estimation of S_{or} can now be developed. In the analysis the convection effect is considered in terms of wave propagation speeds. The difference in accumulation capacities of the medium for different dependent variables causes chromatographic separation at any given convective condition. Therefore the ratio of accumulation capacity for temperature to accumulation capacity for concentration of primary tracer is the potential for separation (abscissa of Figure 11). The value of unity corresponds to no separation. In real SWCT test environments the accumulation capacity for heat is normally larger than that for the primary tracer. Thus only ratios greater than unity are considered in Figure 11.

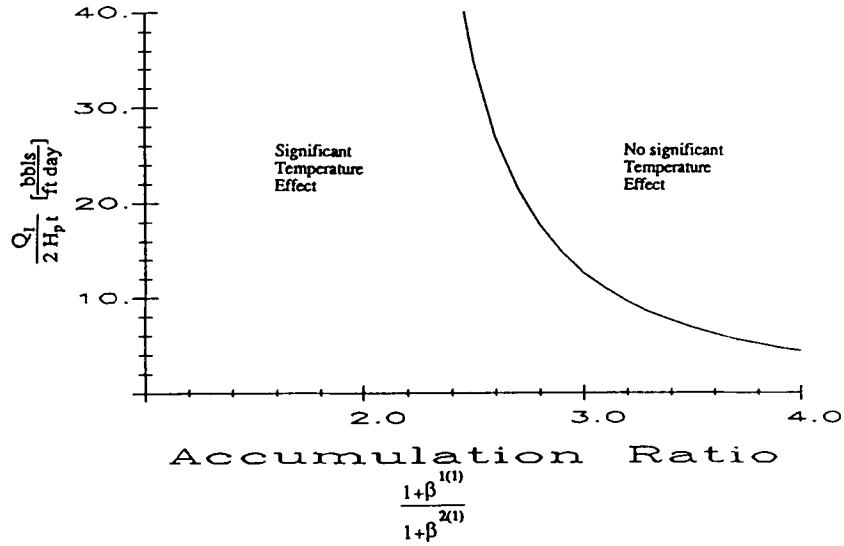

Figure 11. Region of significant temperature effect versus accumulation ratio for the pore diffusion model

The temperature front and tracer bank will be separated while flowing (injecting) if the ratio is greater than unity. Thus the amount of push fluid, which determines the radius of penetration, is also a measure of separation (ordinate of Figure 11).

The thermal diffusion effect is accounted for in terms of the penetration depth. The effect of dispersion of the primary tracer due to the presence of dead-end pore space is quantified by numerical experiments. In Figure 11 the parameter domain for SWCT tests is divided into safe and unsafe regions, relative to temperature effects on the estimation of S_{or} in the medium range of $\gamma^{2(3)}$. In the safe region the estimated values of S_{or} from the non-isothermal and isothermal simulations are essentially the same. This information is very useful to determine when the expensive non-isothermal model needs to be used. Details appear in References 6 and 7.

Two field tests, a Devonial Reef Test (test 7 in Reference 10) and a Mississippian Reef Test (test 1 in Reference 4), were rematched using the non-isothermal simulator. Input data to the simulator and the procedures for obtaining best-fit values of S_{or} were detailed in Reference 6. Tracer production profiles are plotted in Figures 12 and 13. The residual oil saturation values obtained from the isothermal and non-isothermal simulations are compared in Table IV.

5. CONCLUDING REMARKS

Heterogeneous equations in a mixed co-ordinate system have been solved using the finite element method. The variational formulations for the flux terms which control the continuity conditions for the dependent variables between the external and internal domains have been described for two cases: a simply connected internal domain and a case with multiple independent internal domains. For the first case the variational formulation can be generally derived and applied for any dimension and shape of internal domain and surface. An example is shown which gives the temperature distribution in a wellbore (the wellbore model).

When the internal domain is composed of many independent spaces, the projection of the interpolation function of the internal domain to the external domain is assumed to be a delta

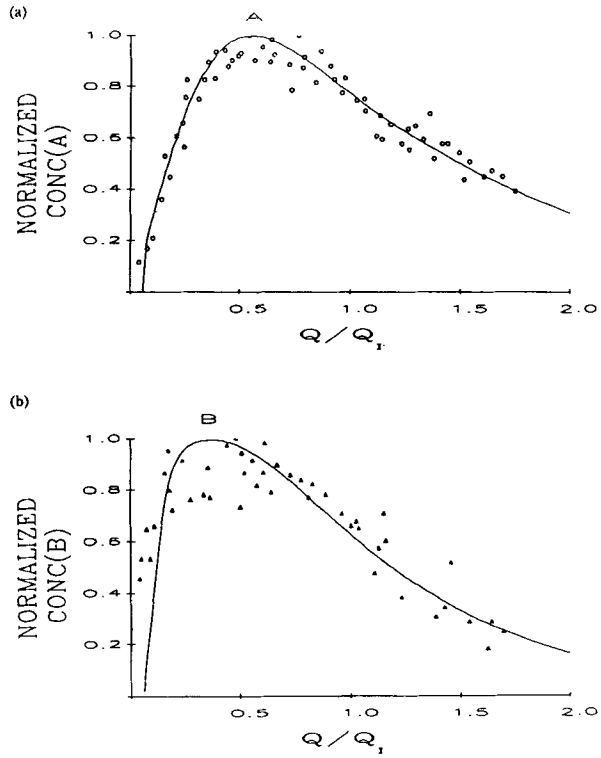

Figure 12. Devonial Reef Test: (a) tracer A; (b) tracer B

Table IV. Estimated residual oil saturations for two field tests

Field Test	Residual oil saturation	
	Non-isothermal	Isothermal
Devonial Reef Test	0·17	0·14
Mississippian Reef Test	0·47	0·42

function in order to maintain independence. Two field tests in heterogeneous carbonate formations are resimulated using this formulation. Residual oil saturation values estimated from this non-isothermal simulation are three to five pore volume per cent higher than those obtained from isothermal simulations. This model has many other applications in the chemical engineering field, such as in adsorption columns, heterogeneous reactors, transport in heterogeneous porous media, etc.

The effect of temperature variation on the determination of residual oil saturation by the single-well chemical tracer test has been bounded using the second type of formulation. The

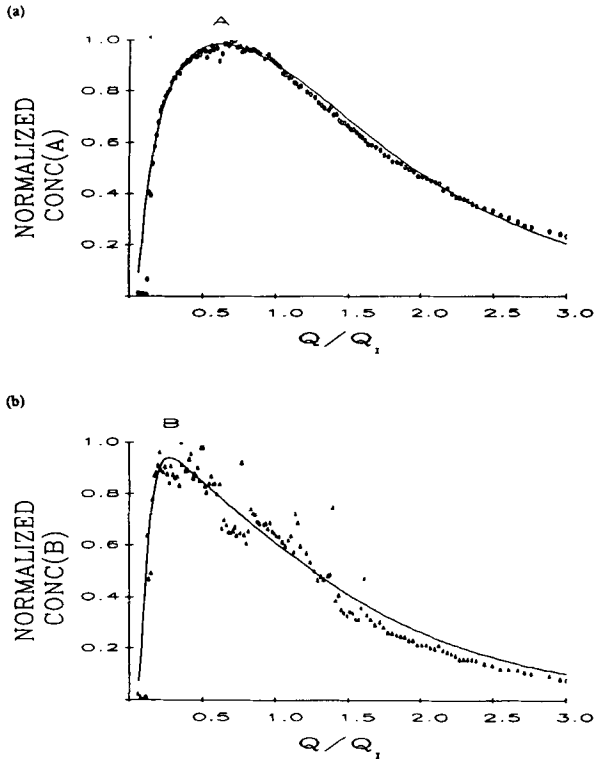

Figure 13. Mississippian Reef Test: (a) tracer A; (b) tracer B

significance of the temperature effects has been analysed in terms of potential for chromatographic separation and the value of the effective push volume. When the reactive tracer bank is separated from the temperature front, so that the tracer bank is located in an isothermal zone after injection has been completed, the temperature effect on the estimation of residual oil saturation does not occur. If the tracer bank and temperature gradient are co-located, the temperature effects can be significant.

ACKNOWLEDGEMENTS

We acknowledge the support of the Enhanced Oil Recovery Laboratory at the University of Houston (to support Y. J. Park) and NSF Grant MSM-8796352 (to support T. E. Tezduyar).

APPENDIX I: THE NON-ZERO TERMS IN EQUATION (4)

The wellbore model

$$\beta^{1(1)} = (\rho c)_w - 1,$$

$$u_1^{1(1)} = q(\rho c)_w/\pi(R_w)^2,$$

$$F^{1(1)} = -a(\gamma^{1(2)}\nabla^2\psi^{1(2)})\cdot\mathbf{n},$$

$$\beta^{1(2)} = (\rho c)_\gamma - 1,$$
$$\gamma^{1(2)} = \mathbf{K}_r,$$
$$a = 2/R_w.$$

The pore diffusion model

$$u_1^{1(1)} = \frac{q}{4\pi H_p \phi (1-(S_o)_{avg}) r},$$

$$u_1^{2(1)} = u_1^{3(1)} = \frac{q}{4\pi H_p \phi (1-S_o^{(1)})(1-f) r},$$

$$\beta^{1(1)} = \frac{\phi(\rho c)_o S_o^{(1)} + (1-\phi)(\rho c)_r}{\phi(\rho c)_w (1-S_o^{(1)})},$$

$$\beta^{1(2)} = \left(\frac{(\rho c)_r}{\phi(\rho c)_w (1-S_o^{(1)})} - 1 \right),$$

$$\beta^{I(\mu)} = \frac{K^I S_o^{(\mu)}}{1-S_o^{(\mu)}} \quad \text{(except for } \beta^{1(1)} \text{ and } \beta^{1(2)}\text{)},$$

$$\gamma = \frac{\mathbf{K}_{r+f}}{\phi(\rho c)_w (1-S_o^{(1)})},$$

$$\gamma^{1(2)} = \frac{\mathbf{K}_r}{\phi(\rho c)_w (1-S_o^{(1)})},$$

$$\gamma^{I(1)} = \gamma^{I(1)}\mathbf{I} = \alpha_d^I u_1^{I(1)}\mathbf{I} \quad \text{for } I = 2, 3,$$

$$R^{2(\mu)} = -R^{3(\mu)} = (10)^{k_0 + E/T} \psi^{2(\mu)} \quad \text{for } \mu = 1, 3,$$

$$F^{I(1)} = a\gamma^{I(3)} \left(\frac{\partial \psi^{I(3)}}{\partial y} \right)_{y=0} \quad \text{for } I = 2, 3,$$

$$(S_o)_{avg} = (1-f) S_o^{(1)} - f S_o^{(3)},$$

$$a = \frac{f(1-S_o^{(3)})}{l(1-f)(1-S_o^{(1)})}.$$

APPENDIX II: NOTATION

c	heat capacity
f	stagnant pore volume fraction
$\mathbf{I}$	identity matrix
K	distribution coefficient
l	average length of dead-end pores
Q	flow volume
R	gas constant
S	saturation
E	activation energy
H_p	half-height of porous formation

k_0 reaction rate constant
$\mathbf{K}$ thermal conductivity
q volumetric flow rate
Q_I injection volume
R_w radius of wellbore

Greek

α_d dispersion parameter
ϕ porosity
ρ density

Superscripts and subscripts

A primary tracer
o oil phase
r+f rock + fluid (oil and water)
B secondary tracer
r rock
w water phase

Conventions for the superscripts and subscripts

β^i ith component of array β
$(\beta)^i$ ith power of β
$u_j^{I(\mu)}$ I = degree of freedom counter, $I = I_{\text{dofb}}^{(\mu)}, \ldots, I_{\text{dofe}}^{(\mu)}$
μ = material number counter, $\mu = 1, \ldots, n_{\text{mat}}$
j = space dimension counter, $j = 1, \ldots, n_{\text{sd}}^{(\mu)}$
$\Omega_k^{(\mu)}$ k = independent space counter, $k = 1, \ldots, n_{\text{pl}}$

REFERENCES

1. H. A. Deans, 'Method of determining fluid saturation in reservoirs', *U.S. Patent 3,623,842*, November 1971.
2. J. F. Tomich, R. L. Dalton, H. A. Deans and L. K. Shallenberger, 'Single-well tracer method to measure residual oil saturation', *J. Petrol. Technol.*, 211–218 (February 1973).
3. T. E. Tezduyar, Y. J. Park and H. A. Deans, 'Finite element procedures for time-dependent convection–diffusion–reaction systems', *Int. j. numer. methods fluids*, **7**, 1013–1033 (1987).
4. H. A. Deans and C. T. Carlisle, 'Single-well tracer test in complex pore systems', *Paper SPE 14886, SPE/DOE Symp. on Enhanced Oil Recovery*, Tulsa, OK, 20–23 April 1986.
5. F. J. M. Horn, 'Calculation of dispersion coefficients by means of moments', *AIChE J.*, **17**, 613–620 (1971).
6. Y. J. Park, H. A. Deans and T. E. Tezduyar, 'Thermal effects on single-well chemical tracer tests for measuring residual oil saturation', *Paper SPE 19683, 64th Ann. Conf. and Exhibition of the Society of Petroleum Engineers*, San Antonio, TX, 8–11 October 1989.
7. Y. J. Park, 'Thermal effects on single-well chemical tracer tests', *Ph.D. Dissertation*, University of Houston, August 1989.
8. T. E. Tezduyar and Y. J. Park, 'Discontinuity capturing finite element formulations for nonlinear convection/diffusion/reaction equations', *Comput. Methods Appl. Mech. Eng.*, **59**, 307–323 (1986).
9. T. J. R. Hughes, *The Finite Element Method, Linear Static and Dynamic Finite Element Analysis*, Prentice-Hall, Englewood Cliffs, NJ, 1987.
10. H. A. Deans and S. Majoros, 'The single-well chemical tracer method for measuring residual oil saturation, Final report', *DOE/BC/20006–18*, October 1980.